



Universiteit
Leiden

The Netherlands

Tuning in to star-planet interactions at radio wavelengths

Kavanagh, R.D.

Citation

Kavanagh, R. D. (2022, November 15). *Tuning in to star-planet interactions at radio wavelengths*. Retrieved from <https://hdl.handle.net/1887/3485841>

Version: Publisher's Version

License: [Licence agreement concerning inclusion of doctoral thesis in the Institutional Repository of the University of Leiden](#)

Downloaded from: <https://hdl.handle.net/1887/3485841>

Note: To cite this publication please use the final published version (if applicable).

3 | Radio eclipses of exoplanets by the winds of their host stars

3.1 Abstract

The search for exoplanetary radio emission has resulted in zero conclusive detections to date. Various explanations for this have been proposed, from the observed frequency range, telescope sensitivity, to beaming of the emission. In a recent paper, we illustrated that exoplanets can orbit through the radio photosphere of the wind of the host star, a region that is optically thick at a specific frequency, for a large fraction of their orbits. As a result, radio emission originating from the planet could be absorbed or ‘eclipsed’ by the wind of the host star. Here we investigate how the properties of the stellar wind and orbital parameters affect the fraction of the orbit where the planet is eclipsed by the stellar wind. We show that planets orbiting stars with low density winds are more favourable for detection in the radio. In terms of the orbital parameters, emission from transiting planets can escape the stellar wind easiest. We apply our model to the τ Boo planetary system, and show that observing the fraction of the planet’s orbit where it is eclipsed by the wind of the host star could be used to constrain the properties of the stellar wind. However, our model developed would need to be used in conjunction with a separate method to disentangle the mass-loss rate and temperature of the stellar wind.

3.2 Introduction

Over the last few decades, the search for exoplanetary radio emission has been motivated by the desire for a new method of directly detecting exoplanets. In addition to this, if the mechanism driving the planetary radio emission is due to interactions with the planet’s intrinsic magnetic field, detection of exoplanetary radio emission would allow us to assess the strength of the planet’s magnetic field (Zarka et al., 2001). This has consequences on the size of the planet’s magnetosphere, which in turn can effect the lifetime of the planet’s atmosphere. Whether this has a positive or negative effect is still in debate (Blackman & Tarduno, 2018; Carolan et al., 2019; Egan et al., 2019).

Despite many attempts, there have been no conclusive detections of exoplane-

tary radio emission to date (e.g. Lazio et al., 2010b; Sirothia et al., 2014; O’Gorman et al., 2018). Some possible explanations for this include the frequency range of the observations, the telescope sensitivity, the atmosphere of the planet (Weber et al., 2018; Daley-Yates & Stevens, 2018), and the emission not being beamed in the direction of the observer (Smith et al., 2009). Another possible explanation for this was made by Kavanagh et al. (2019), who illustrated that exoplanets can orbit through the radio photosphere of the winds of their host stars, a region where a large fraction of radio emission can be absorbed through free-free processes. As the radio photosphere is not spherically symmetric, when the planet orbits further into the wind of the host star more of its emission can be absorbed.

There have been hints of a decrease in the flux density at radio frequencies from transiting exoplanets near secondary transit. Smith et al. (2009) observed this in the case of hot Jupiter HD189733b. Similarly, observations of HAT-P-11b system by Lecavelier des Etangs et al. (2013) suggested a dip in the flux density near secondary transit. However, these results are inconclusive, and require follow-up observations with more sensitive instrumentation (Smith et al., 2009; Lecavelier des Etangs et al., 2013; Sirothia et al., 2014). If confirmed, these dips in flux density near secondary transit could be due to the stellar wind of the host star absorbing the emission from the planet, as suggested by Kavanagh et al. (2019).

A similar illustration of this phenomenon is the case of Black Widow pulsar systems (Roberts, 2011). These systems consist of a millisecond pulsar that is host to a low-mass companion with a mass of $\sim 0.01 M_{\odot}$. As the companion nears primary transit of the pulsar host, radio emission originating from the pulsar is observed to disappear (see Polzin et al., 2019). This is believed to be due to the wind of the low-mass companion star eclipsing the pulsar. For example, Guillemot et al. (2019) observed eclipses of radio emission at 1.4 GHz from the Black Widow pulsar PSR J2055+3829. Due to the time variations of the eclipse, this has been attributed to the clumpy outflow of the companion star.

Radio eclipses have been observed in higher mass binaries as well. For example, Dougherty et al. (2005) observed a similar phenomenon in the massive binary system WR140. From VLBA observations at 8.4 GHz they resolved that radio emission generated from the collision of the winds of the two stars in the system disappears as the O-type star approaches periastron of the Wolf-Rayet star. This has been interpreted as the emission region entering the optically thick region of the wind of the Wolf-Rayet star.

In this paper, we present a model that predicts that radio emission from the planet becomes eclipsed by the wind of the host star as the planet progresses through its orbit. We illustrate how the properties of the wind of the host star and the planetary orbit affect the duration of the radio eclipse, and then apply our model to the τ Boo planetary system. We show how the model presented could be used to constrain properties such as the mass-loss rate and temperature of the stellar wind of the host star.

3.3 Radio eclipse of the planet by the stellar wind

To model the wind of the host star, we consider only forces due to the gravity of the star and the thermal pressure gradient of the wind (Parker, 1958):

$$\rho u \frac{d}{dr} u = -\frac{\rho G M_\star}{r^2} - \frac{d}{dr} p. \quad (3.1)$$

Here, ρ is the mass density, u is the velocity, r is the distance, G is the gravitational constant, M_\star is the mass of the star, and p is the thermal pressure. Assuming that the stellar wind is isothermal and mass is conserved, Equation 3.1 can be re-arranged into the following form:

$$\frac{1}{u} \frac{d}{dr} u = \left(\frac{2a^2}{r} - \frac{GM_\star}{r^2} \right) / (u^2 - a^2), \quad (3.2)$$

where a is the isothermal sound speed:

$$a = \sqrt{\frac{k_B T}{\mu m_p}}. \quad (3.3)$$

Here, k_B is Boltzmann's constant, T is the wind temperature, and μm_p is the mean mass per particle in the stellar wind, with m_p being the proton mass. For a fully ionised hydrogen wind, we take $\mu = 1/2$.

We solve Equation 3.2 enforcing a solution that passes through the critical point, where the numerator and denominator on the right-hand side go to zero simultaneously. This is to ensure a wind solution is obtained which monotonically increases in velocity outward (Parker, 1958). Such a critical point occurs at the sonic distance

$$r_c = \frac{GM_\star}{2a^2}, \quad (3.4)$$

where the velocity of the wind at the critical point is $u = a$. Note that a physical solution is one where r_c is greater than the stellar radius. With that, we obtain the wind velocity profile for a given stellar mass M_\star and wind temperature T . The mass-loss rate of the stellar wind is

$$\dot{M} = 4\pi r^2 \rho u. \quad (3.5)$$

So, for a given stellar mass, wind temperature and mass-loss rate, we obtain a mass number density profile of the stellar wind:

$$n = \frac{\dot{M}}{4\pi r^2 \mu m_p u}. \quad (3.6)$$

One of the benefits of using a 1D isothermal stellar wind model is that it is much less time consuming than performing a 3D magnetohydrodynamic stellar wind simulation, such as those computed by Kavanagh et al. (2019). A limitation of isothermal stellar wind models is that they neglect the presence of a magnetic

field, which is important for determining the angular momentum-loss rates and therefore the rotational evolution of low-mass stars (Weber & Davis, 1967; Réville et al., 2015; Johnstone et al., 2015; Ó Fionnagáin et al., 2019a). However, as we do not consider an evolving stellar wind here, we assume that an isothermal stellar wind model is sufficient for our purposes in this paper.

As the planet progresses further into its orbit, the amount of stellar wind material between the planet and observer increases. Since the wind of the host star can absorb low-frequency radio emission through free free processes (Panagia & Felli, 1975), a larger fraction of radio emission from the planet will be absorbed as it approaches an orbital phase of $\phi = 0.5$. We refer to a region of the stellar wind at a specific frequency as the ‘radio photosphere’, wherein only a certain fraction (i.e. 50%) of radio emission can escape through the wind. This is illustrated in the top panel of Figure 3.1. Note that there is one further complication: if the plasma frequency of the stellar wind at the planet’s orbit

$$\nu_p = 9 \times 10^{-3} \sqrt{n_e} \text{ MHz} \quad (3.7)$$

is greater than the emitted frequency from the planet ν , no emission will generate. Here, n_e is the electron number density of the local stellar wind in cm^{-3} .

We do not model the emission mechanism of the planet here, but rather how such an emission, if existed, would be absorbed by the wind of the host star. We also assume that the emission from the planet is always beamed towards the observer. To determine how much planetary emission is absorbed by the stellar wind, we compute the optical depth at frequency ν at the planet’s position x_p along the line of sight in the stellar wind (see Figure 3.1):

$$\tau_\nu = \int_{-\infty}^{x_p} \alpha_\nu dx. \quad (3.8)$$

Here, α_ν is the free-free absorption coefficient (Cox, 2000):

$$\alpha_\nu = 3.692 \times 10^8 \left(1 - e^{-h\nu/k_B T}\right) Z^2 g T^{-1/2} \nu^{-3} n_e n_i, \quad (3.9)$$

where h is Planck’s constant, Z is the ionisation state (+1 for ionised hydrogen), and g is the Gaunt factor (Cox, 2000):

$$g = 10.6 + 1.9 \log_{10}(T) - 1.26 \log_{10}(Z\nu). \quad (3.10)$$

In Equation 3.9, n_e and n_i are the electron and ion number densities respectively. Since we treat the wind as being composed of fully ionised hydrogen, the total number density is $n = n_e + n_i = 2n_e$ ($n_e = n_i$). The ion number density is the proton number density in this case.

The observer receives a specific intensity I_ν at frequency ν from the planet that has been attenuated by the stellar wind (Rybicki & Lightman, 1986):

$$I_\nu = I_{\nu,0} e^{-\tau_\nu}, \quad (3.11)$$

where $I_{\nu,0}$ is the emitted specific intensity by the planet. This is illustrated in the bottom panel of Figure 3.1. The flux density received by the observer is then:

$$F_{\nu} = \int I_{\nu} d\Omega = \frac{1}{d^2} \int I_{\nu} dA, \quad (3.12)$$

where $d\Omega$ is the element of solid angle of the emitting region, d is the distance to the system, and dA is the area element of the emitting region. Assuming that the specific intensity I_{ν} is constant through dA , then from Equations 3.11 and 3.12:

$$F_{\nu} \propto e^{-\tau_{\nu}}. \quad (3.13)$$

So, if $F_{\nu,0}$ is the flux density one would observe in the absence of a stellar wind, the observed flux density from the planet is:

$$F_{\nu} = F_{\nu,0} e^{-\tau_{\nu}}. \quad (3.14)$$

The term $e^{-\tau_{\nu}}$ therefore gives the fraction of the flux density that is transmitted from the planet to the observer. When computing the optical depth at each point in the planet's orbit with Equation 3.8, we extend the stellar wind out from the planet to a distance of 0.5 au in the direction of the observer ($-x$ direction). This distance is sufficient for the optical depth at the planet's position to converge.

Figure 3.2 illustrates how emission from a transiting planet orbiting its host star disappears as it approaches secondary transit. In this example, the planet orbits a star with a mass of $1 M_{\odot}$ and radius of $1 R_{\odot}$ at 0.02 au. The wind of the host star has a mass-loss rate of $100 \dot{M}_{\odot}$, where \dot{M}_{\odot} is the solar wind mass-loss rate ($2 \times 10^{-14} M_{\odot} \text{ yr}^{-1}$), and a temperature of 2 MK. The left panel shows the combined thermal spectrum of the wind of the star with that of a planet at different orbital phases. We assume that the planet emits an unattenuated flux density of $F_{\nu,0} = 100 \mu\text{Jy}$ in the region of 20-40 MHz. The value of $F_{\nu,0}$ chosen here is purely for illustrative purposes. The thermal spectrum of the stellar wind is computed as per the method laid out in Ó Fionnagáin et al. (2019a) and Kavanagh et al. (2019). We compute the spectrum placing the system at 1 pc from the observer.

The right panel of Figure 3.2 shows the number density profile of the stellar wind which the planet orbits through. The orbital phases we compute the spectrum of the planet for in the left panel are marked along the orbit. As the planet progresses through its orbit towards secondary transit ($\phi \gtrsim 0.36$), the flux received from the planet begins to disappear. Past a certain point the wind of the host star eclipses the planet. Towards higher frequencies however, this effect is less pronounced. This was shown by Kavanagh et al. (2019), in that the planet is easier to detect both near primary transit of the host star and at higher emitted frequencies.

3.4 Stellar wind effects on radio eclipses

Here, we investigate how the properties of the stellar wind itself affect how much planetary emission escapes through the wind. Figure 3.3 shows how varying the

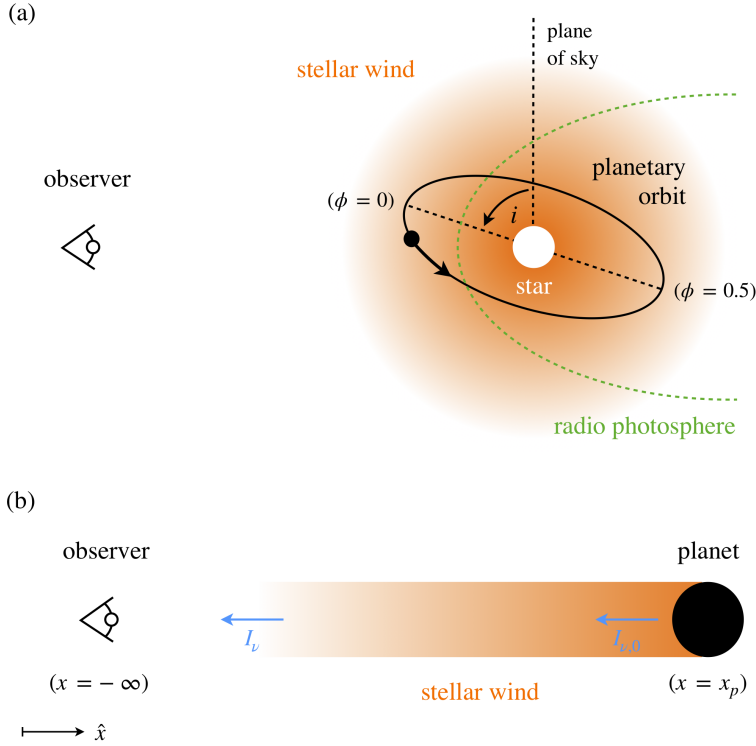


Figure 3.1: *Top*: Sketch illustrating a planet that orbits in a circle through the wind of its host star, inclined at an angle i from the plane of the sky. Orbital phases of $\phi = 0$ and $\phi = 0.5$, corresponding to when the planet is nearest and furthest from the observer respectively, are marked along the orbit. The radio photosphere of the stellar wind is also shown, which the planet orbits through for a fraction of its orbit. *Bottom*: The line of sight radio emission originating from the planet takes through the stellar wind towards the observer. The planet emits a specific intensity of $I_{\nu,0}$, and the observer sees an attenuated specific intensity of $I_\nu = I_{\nu,0}e^{-\tau_\nu}$.

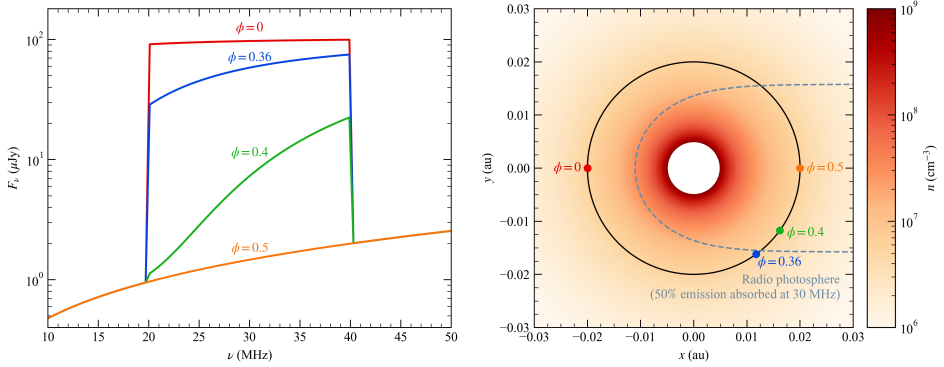


Figure 3.2: *Left*: The combined spectrum of free-free emission from the stellar wind and emission from the planet at different orbital phases. The system is placed at 1 pc for this illustration, with the planet emitting an arbitrary unattenuated flux density of 100 μ Jy. *Right*: Number density profile of the stellar wind, and the positions of the planet corresponding to the spectra shown in the left panel. The dashed line shows the radio photosphere where 50% of emission is absorbed at 30 MHz by the stellar wind. The observer looks towards the system from $x = -1$ pc along the x -direction.

mass-loss rate of the wind of the host star affects the percentage of escaping emission at 30 MHz as the planet progresses through its orbit. As the planet approaches secondary transit of the star (orbital phase of 0.5), the planetary emission becomes eclipsed by the stellar wind. This effect is more pronounced for higher stellar wind mass-loss rates, which in turn are denser for a fixed temperature. Note that at 30 MHz, a low mass-loss rate stellar wind does not attenuate the planetary emission at primary transit ($\phi = 0$). However at higher mass-loss rates, even when the planet transits part of its emission is attenuated and the flux density would not be observed at this frequency.

In Figure 3.4 we show varying how the temperature of the stellar wind, for a fixed mass-loss rate, affects the amount of escaping emission from the planet. We see that detection of exoplanetary radio emission is favoured for high temperature winds, with the eclipse occurring for a smaller fraction of the planet’s orbit. As the wind is accelerated much faster in at higher temperatures, the density of the wind drops off much faster (following from Equation 3.6). As a result, hotter winds tend to be less dense. However, the mass-loss rates of low-mass stars are expected to increase with surface X-ray flux (see Wood, 2018), which in turn is correlated with a hot corona (Johnstone & Güdel, 2015). So while the most favourable detection scenario would be a planet that orbits a star with a hot wind with a low mass-loss rate, it is more likely that if the wind is very hot, the mass-loss rate is high. In general, planets orbiting stars with low density winds are more favourable for detection.

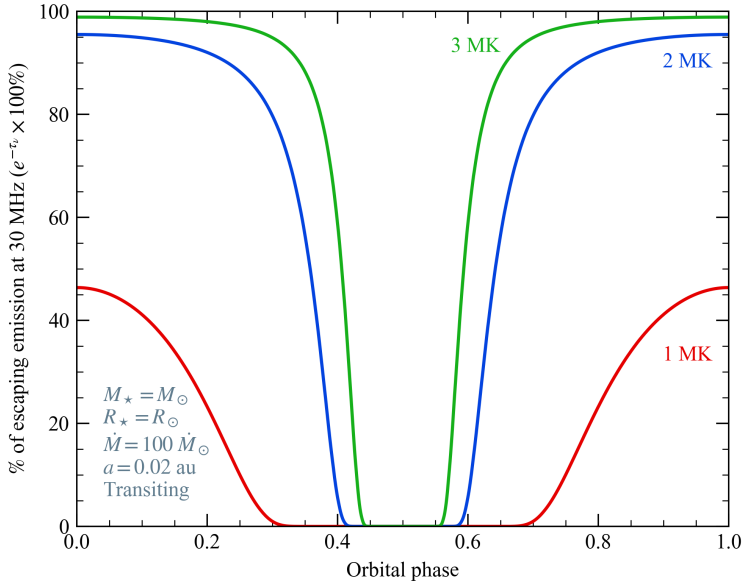


Figure 3.4: Same as Figure 3.3, but for different stellar wind temperatures.

3.5 Orbital effects on radio eclipses

The amount of planetary emission that escapes the wind of the host star also depends on the path it takes as the planet progresses through its orbit. Here, we investigate how the geometry of the orbit affects the duration of the radio eclipses. In Figure 3.5 we show the effects of varying the orbital inclination of the planet. We find that a transiting planet is the most easily detectable, specifically near primary transit ($\phi = 0$). However, in this configuration the planetary emission also is the most attenuated, near secondary transit ($\phi = 0.5$), with the largest amplitude of the eclipse modulation.

The transmitted flux density on the other hand for a planet in a plane of sky orbital configuration is constant, assuming the unattenuated flux density $F_{\nu,0}$ is constant. As a result, a planet orbiting in the plane of the sky will either always be detectable or never be detectable, depending on the instrument sensitivity and the amount of flux that escapes the stellar wind. Detection is also in theory always possible for planets orbiting at inclinations $0 < i < \cos^{-1}(a/R_*)$, as the planet does not pass behind the stellar disk.

Figure 3.6 show the effects of varying the orbital distance of a transiting planet on the amount of escaping emission. We see that the closer in to the star the planet orbits, the lower the amount of emission escapes as the density of the stellar wind is much larger close in. In addition to this, if the stellar wind plasma frequency is too high the emission will not generate. This is the case for a planet orbiting at 0.01 au for the parameters presented in Figure 3.6. So, planets orbiting further

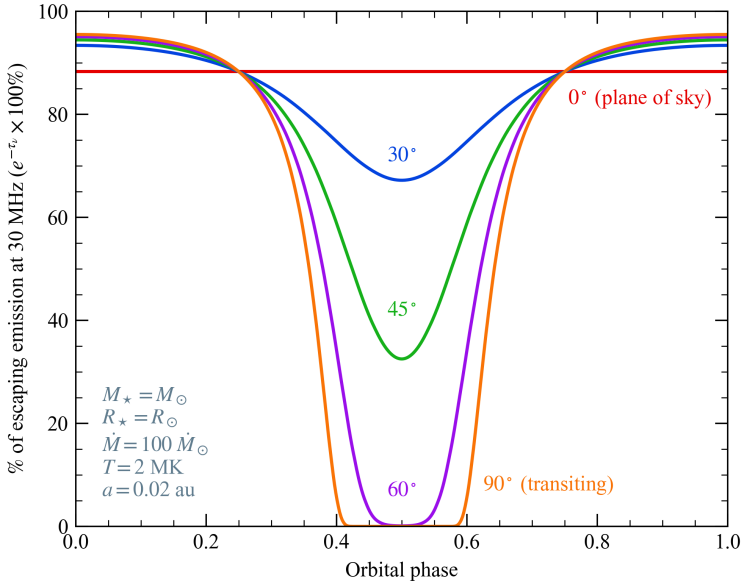


Figure 3.5: Same as Figure 3.3, but for different orbital inclinations. Transiting planets have the most favourable conditions for detection, but also have the largest modulation of their emitted flux density.

out are more easily detectable. However, if the stellar wind power dissipated onto the planetary magnetosphere powers the planetary radio emission, planets further out are likely to emit much lower flux densities than those closer in (Zarka et al., 2001).

3.6 Constraining the stellar wind properties of the hot Jupiter host τ Boo

We now focus on the τ Boo planetary system, which lies 15.6 pc away from Earth. The star is host to the supermassive hot Jupiter τ Boo b which orbits at just 0.046 au, and as a result the planet is expected to be a source of strong radio emission (see Weber et al., 2018). As the planet does not transit its host star ($i = 45^\circ$), in theory it could be detectable for the entirety of its orbit if it emits a high enough flux density, following the results shown in Figure 3.5. The mass and radius of the star are $1.30 M_\odot$ and $1.33 R_\odot$ respectively. All parameters listed above are taken from exoplanet.eu.

As illustrated in Figures 3.3 and 3.4, the amount of escaping emission from the planet depends on the mass-loss rate and temperature of the wind of the host star, both of which are unknowns in the case of τ Boo. Another two unknown quantities of the system are the emitted flux density and frequency from the planet (if it is indeed a source of exoplanetary radio emission). Turner et al. (2019) showed that

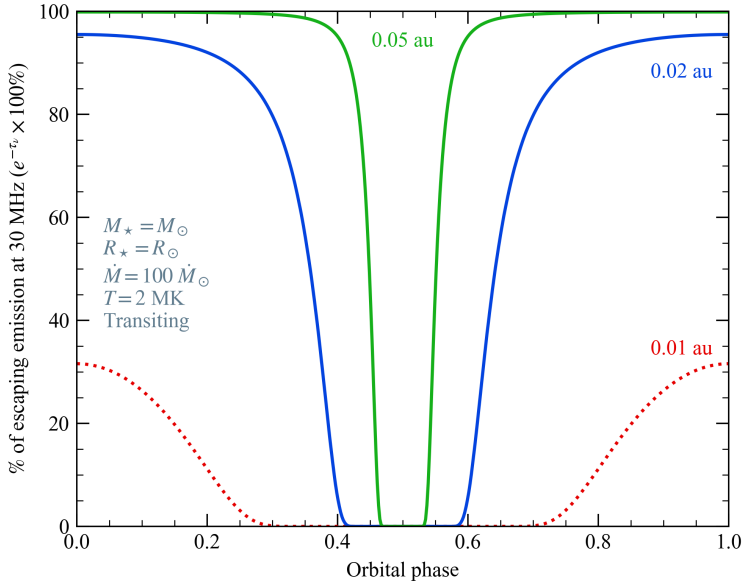


Figure 3.6: Same as Figure 3.3, but for different orbital distances. At 0.01 au, the plasma frequency of the stellar wind at the planet’s is greater than 30 MHz and as a result no emission can generate. This is indicated by the dashed line.

emission from τ Boo b would be detectable with LOFAR, if it emits a flux density that is 10^5 times larger than that emitted by Jupiter. During active periods, Jupiter has an observed flux density 10^7 Jy at a distance of 1 au (Zarka et al., 2004). Therefore, at a distance of 15.6 pc, we assume an unattenuated flux density for τ Boo b of $F_{\nu,0} = 96.6$ mJy.

If we also assume that the planet emits at a frequency of 30 MHz, we can determine for what fraction of the planet’s orbit it would be detectable with LOFAR. At 30 MHz LOFAR has a sensitivity of $F_{\nu}^{\text{LOFAR}} \sim 7$ mJy for a 1 hour integration time (see Figure 1 of Griekmeier et al., 2011). The planet is then detectable when $F_{\nu} > F_{\nu}^{\text{LOFAR}}$ or when $e^{-\tau_{\nu}} > 0.0725$ following Equation 3.14.

Figure 3.7 shows the combination of stellar wind mass-loss rate and temperature that results in detection of emission from τ Boo b at 30 MHz with LOFAR for 25%, 50%, and 75% of its orbit. As can be seen, if emission was detected from the system at 30 MHz for, say, 50% of the planet’s orbit, there is a degeneracy between the stellar wind mass-loss rate and temperature. So while observing radio emission alone from the planet for a certain fraction of its orbit does not provide enough information to derive the stellar wind properties, it could nevertheless be used in conjunction with the radiometric Bode’s law to provide additional constraints (see Vidotto & Donati, 2017). In Figure 3.7 we also show that the plasma frequency of the stellar wind at the planet’s orbit and the maximum temperature of the stellar wind can constrain the parameters of the stellar wind. We derive a maximum coronal temperature (and therefore the wind) for τ Boo of 3.7 MK from

Johnstone & Güdel (2015), using the maximum observed X-ray luminosity for the host star of $8 \times 10^{28} \text{ erg s}^{-1}$ (Mittag et al., 2017).

The mass-loss rates of the winds of low-mass stars have proved to be very difficult to measure, and has only been possible in a handful of cases. One such method relies on observations of the absorption of Ly- α from the star due to the build-up of neutral hydrogen at the astrosphere (Wood, 2004). Vidotto & Bourrier (2017) also illustrated how stellar wind mass-loss rates could be derived based on observations of Ly- α absorption due to the presence of an extended planetary atmosphere. Both of these methods however require Hubble Space Telescope observations, and therefore cannot be carried out for a large number of targets. More recently, Jardine & Collier Cameron (2019) showed how the mass-loss rates of low-mass stars could be derived based on the presence of prominences from H α observations. This method however is only possible for very fast rotators. Mass-loss rates from low-mass stars could also be determined from observations of thermal free-free radio emission from the stellar wind itself (Güdel, 2002), however current radio telescopes are not sensitive enough to detect this emission (Ó Fionnagáin et al., 2019a). Our method presented here could provide a new method of constraining the mass-loss rates of low-mass stars from radio observations with current telescopes (i.e., LOFAR), if combined with another method such as the radiometric Bode’s law.

One of the main issues with the application of our model in this section is that in order to determine when a planet would be detectable with a given radio telescopes, we require knowledge of the unattenuated flux density emitted by the planet. In addition to this, it is likely that the emitted flux density varies over the orbit. This has been shown to be the case if the emission mechanism powering the planetary radio emission is the interaction between the stellar wind and planetary magnetosphere, as the wind of the host star is not uniform (see Figure 4 of Kavanagh et al., 2019; Nicholson et al., 2016). For instance, Jupiter is observed to experience active periods where the flux density emitted increases (Zarka et al., 2004).

3.7 Conclusions

In this work, we have presented how the properties of the stellar wind and the orbital characteristics of a planet affect the fraction of the planet’s orbit where its radio emission is eclipsed by the wind of the host star. We have illustrated that detection of planetary radio emission is favoured for host stars with low density winds. The ideal case for this would be a star with a hot wind and low-mass loss rate, however low-mass stars with hot winds generally have high mass-loss rates.

In terms of orbital parameters, emission can most easily escape the wind of the host star for transiting planets, specifically in the region near primary transit. However, in this orbital configuration, the emission is also most attenuated near secondary transit. Therefore, transiting exoplanets offer the most extreme case in which radiation escapes the most ($\phi = 0$) or is most attenuated ($\phi = 0.5$). Planets with orbital inclinations in the range $0 < i < \cos^{-1}(a/R_\star)$ can in theory always be

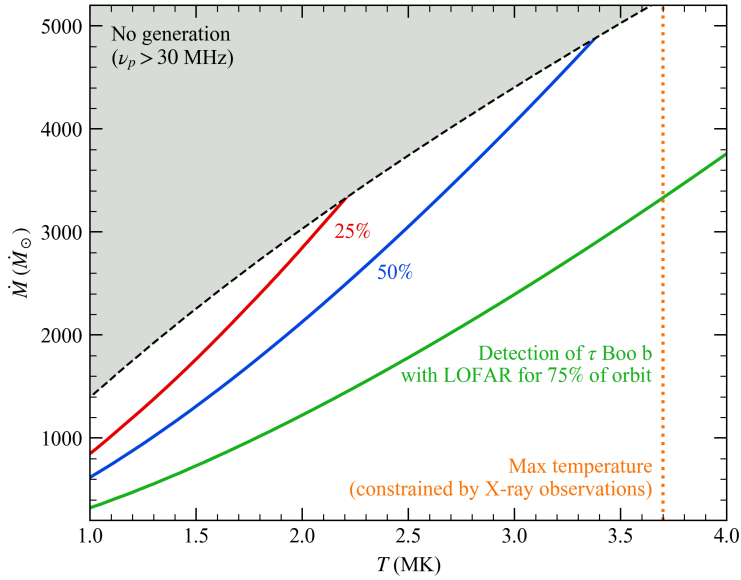


Figure 3.7: The combined stellar wind mass-loss rate and temperature that results in detection of radio emission from τ Boo b at 30 MHz with LOFAR, for 25%, 50%, and 75% of its orbit. The shaded area illustrates where the plasma frequency of the stellar wind at the planet’s orbit is too high for generation of radio emission at 30 MHz. The vertical dotted line marks the maximum temperature of the stellar wind, which is constrained by X-ray observations of the host star (see relevant text).

detected, depending on the emitted flux density and density of the stellar wind, as they do not pass behind the stellar disk. We also have illustrated that planets orbiting closer to their host stars are less likely to be detected, as the stellar wind is very dense close in. However, if the planet orbits far out from its host star, the mechanism powering the radio emission of the planet may be too weak (see Zarka et al., 2001).

We applied our model to the τ Boo planetary system, and illustrated that if radio emission is detected from the planet for a certain percentage of the orbit with LOFAR, we can constrain the wind properties of the host star. Observations such as this are not sufficient to disentangle the mass-loss rate and temperature of the wind. In combination with another method however such as the radiometric Bode’s law could help to further constrain the stellar wind properties. The plasma frequency of the stellar wind as well as X-ray observations of the host star could also aid constraining the wind properties.

Acknowledgements

RDK acknowledges funding received from the Irish Research Council through the Government of Ireland Postgraduate Scholarship Programme. AAV acknowledges funding from the Irish Research Council Consolidator Laureate Award 2018 and the European Research Council (ERC) under the European Union’s Horizon 2020 research and innovation programme (grant agreement No 817540, ASTROFLOW).